COMMUNICATIONS PHYSICS

ARTICLE

DOI: 10.1038/s42005-018-0025-4 OPEN

Spatiotemporal control of cargo delivery performed by programmable self-propelled Janus droplets

Menglin Li[1], Martin Brinkmann[1], Ignacio Pagonabarraga[2], Ralf Seemann[1] & Jean-Baptiste Fleury[1]

Self-propelled droplets capable of transporting cargo to specific target locations are desired tools for many future applications. Here we propose a class of active droplets with programmable delivery time that are attracted or repelled by certain obstacle geometries. These droplets consist of a water/ethanol mixture and are dispersed in an oil/surfactant solution. Owing to a mass exchange between fluid phases during self-propulsion, the initially homogeneous droplets spontaneously de-mix and evolve into characteristic Janus droplets. Cargo molecules, like DNA, can be separated into the trailing ethanol-rich droplet and are carried to their target location "like in a backpack". The delayed onset of phase separation provides a handle to control the time frame of delivery, while long-ranged hydrodynamic interactions and short-ranged wetting forces are exploited to achieve the desired spatial specificity with respect to obstacle geometry and surface chemistry.

[1] Universität des Saarlandes, Experimental Physics, 66123 Saarbrücken, Germany. [2] Department of Condensed Matter Physics, University of Barcelona, Carrer de Marti I Franques 1, 08028 Barcelona, Spain. Correspondence and requests for materials should be addressed to M.B. (email: martin.brinkmann@physik.uni-saarland.de) or to R.S. (email: ralf.seemann@physik.uni-saarland.de) or to J.-B.F. (email: jean-baptiste.fleury@physik.uni-saarland.de)

In recent years, significant efforts were dedicated to realize artificial micro-swimmers and nano-swimmers that locomote at low Reynolds numbers, and that are further able to perform tasks, like cargo delivery[1–3]. Micro-swimmers driven by periodic conformational changes have to break the time-reversal symmetry to achieve a net propulsion in the Stokes regime[4,5]. However, micro-swimmers driven by a continuous propulsion mechanism need to break spatiotemporal symmetry and display a permanent polarity. Despite the theoretical possibility to observe a spontaneous symmetry breaking for homogeneous spherical particles[6], all solid autophoretic micro-swimmers realized in experiments so far are polar already by their design. Spherical Janus particles, for instance, exploit a difference in chemical surface composition of the two opposing hemispheres[7].

Recent studies have shown that Janus nanorods can not only self-propel but also deliver drugs during self-propulsion[8], repair cracks in electrical circuits[9], or even halt blood hemorrhages[2]. Besides their desired properties, the chemical composition of these colloidal (Janus) particles and the underlying process of their self-propulsion often excludes the use in biotechnological applications[1]. Emulsion droplets, in contrast, have the potential to be composed of bio-compatible liquids. It was also shown that emulsion droplets can self-propel by Marangoni stresses[10] that are maintained by chemical reactions[11], micellar solubilization[12,13], or liquid–liquid phase separations[14–19]. However, the realization of self-propelled Janus droplets has been proven difficult[20–24] in spite of the achievements obtained with emulsion droplets. Swimming droplets could so far not perform tasks comparable to self-propelling solid particles.

In this article, we report time-evolutive self-propelled water/ethanol droplets in an ambient oil surfactant solution, with the ability to deliver cargo (here DNA) in a single step. The evolution of the emulsion droplets is caused by a continuous release of ethanol from the droplet into the ambient phase and a simultaneous uptake of surfactant. After a certain time, the surfactant concentration in the droplet reaches the threshold value for a spontaneous phase separation into a water-rich and an ethanol-rich phase forming a Janus droplet, which continues to self-propel. The duration of the evolution stages and the transport distances can be controlled by droplet size and ethanol concentration, while the specific hydrodynamic flow fields emerging during each evolution stage and the specific wetting conditions of the target location, enabling an unprecedented spatiotemporal control of cargo delivery.

Results

The generation of evolutive self-propelling droplets can be achieved using a four component system consisting of water, a water-miscible solvent being less polar than water and partially soluble in the surrounding oily phase, and an oil soluble surfactant. Further, the surfactant needs a chemical affinity for the solvent and the oil should be immiscible with water. A combination of chemical substances satisfying all these conditions is water/ethanol/monoolein and squalane (4% of ethanol is soluble in squalane). For simplicity we will restrict the following description to this particular system with a monoolein concentration of 10 mM if not explicitly mentioned otherwise, but the reported concept is universal and similar results can be obtained also for other combinations of alcohols, oils, and amphiphilic molecules as detailed in the Supplementary Information.

Evolution stages. Water/ethanol droplets (with typical radii in the range between 35 and 80 μm) are injected into an ambient squalane/monoolein solution and evolve in up to three different stages during self-propulsion (Fig. 1).

For intermediate ethanol concentrations, between 40 and 60 vol%, the droplets self-propel immediately after their

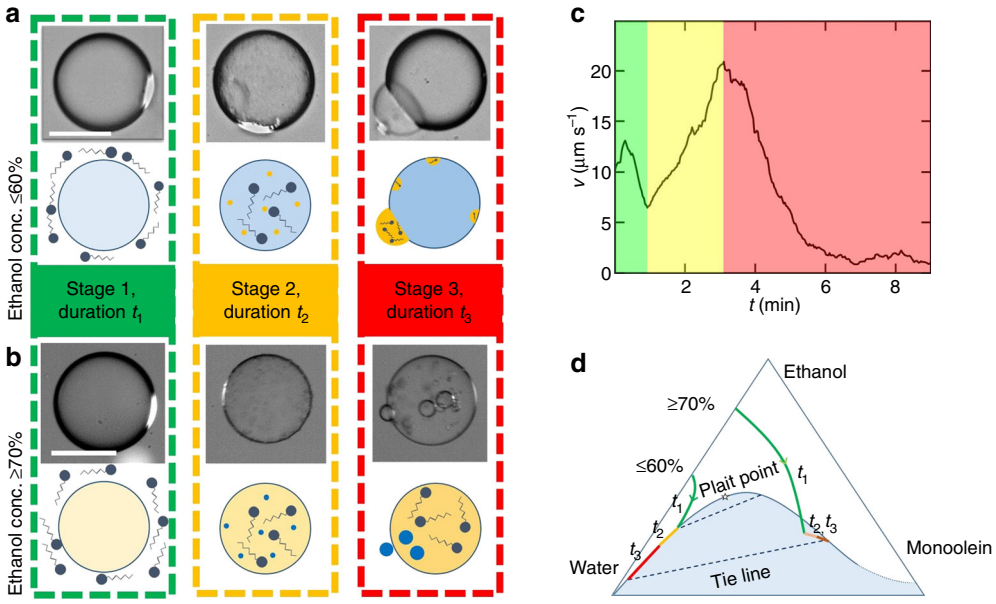

Fig. 1 Evolution stages of self-propelling water/ethanol emulsion droplets for ethanol concentrations between **a** 30 and 60 vol%. Top rows display optical micrographs and second row sketches. The color intensity of the sketches indicate increasing concentration of water, respectively, ethanol. (Stage 1) ethanol solubilization and uptake of surfactant molecules. (Stage 2) nucleation and coalescence: phase separation into a water-rich and an ethanol-rich phase that contains most of the surfactant molecules. (Stage 3), formation of long or short-lived Janus droplets. Scale bar is 100 μm. **b** For ethanol concentrations ≳70 vol% small water-rich droplets are formed, which are expelled from the ethanol-rich majority phase. Droplet velocities as function of time for initial ethanol concentrations of **c** ~50 vol%, where droplets can be observed in all stages but stage 1 is relatively short, and **d** sketch of the ternary phase diagram of water/ethanol/monoolein. Tentative pathways for two initial concentrations (of ≳70 and ≲60 vol%) are displayed

production (stage 1). Depending on ethanol concentration the droplet phase de-mixes after 20–300 s and small droplets appear in the bulk of the self-propelling droplet (stage 2). The average radius of these small droplets grows, eventually leading to the formation of a single droplet, which is pushed out of the self-propelling droplet and trails behind (Fig. 1a). This stage 2 lasts for about 1–2 min, while the emerging droplets constitute a long-lived Janus droplet that self-propels for about ≈5 min (stage 3) before the droplets separate. After separation, the trailing droplet typically spreads on the hydrophobic container bottom while the leading droplet stops its motion gradually after moving a few droplet radii (Supplementary Movie 1). During these different stages, the corresponding hydrodynamic flow field around the droplets could be measured by Micro-Particle Image Velocimetry (μPIV) (Fig. 2).

For water/ethanol droplets with a small initial ethanol concentration of about 30 vol%, the de-mixing starts almost immediately after droplet production, and thus the droplets self-propel almost immediately in stage 2. However, as also the de-mixing in stage 2 is fast, the self-propulsion can effectively be observed only in stage 3 for about 5 min. Reducing the initial ethanol concentration in the droplets below 30 vol%, de-mixing is not always observed and self-propelled motion does not occurr reliably. Droplets prepared with an ethanol concentration between 70 and 80 vol% show all three evolution stages (Fig. 1b). For such high ethanol concentrations the duration of stage 1 is extended to 10–15 min. The subsequent de-mixing in stage 2 occurs within 1–2 min. But in contrast to intermediate and low ethanol concentrations, the small droplets, which emerge inside the self-propelling droplet in the course of stage 2, finally separate from the larger droplet and continue to self-propel while the larger droplet spreads on the hydrophobic container bottom and stops moving (stage 3). Droplets with ethanol concentrations above 80 vol% spread easily on the container bottom and are hard to observe; we thus restrict our quantitative consideration to a maximum ethanol concentration of 80 vol%.

During self-propulsion in stage 1 the droplets loose volume, and as ethanol is soluble and water is insoluble in squalane we expect that ethanol is released from the droplet phase. In fact the droplets release more material with increasing ethanol concentration, which is visible by the reduction of droplet volume ranging from only a few percent at 30 vol% ethanol concentration to about 40% volume loss for an ethanol concentration of 80 vol %. The droplet velocities in stage 1 vary roughly around 10 μm s $^{-1}$ (Fig. 1c) independent of ethanol concentration and droplet size. The propulsion time t_1 and with it the cruising range in stage 1 increase significantly with ethanol concentration (Fig. 1d) and (Fig. 3a), which can be regarded as the "fuel" for this propulsion process. Similarly, t_1 and the cruising range increase also with droplet size, i.e., with increased ethanol availability (Fig. 3b, c). Hence, droplets travel the further in stage 1 the larger their ethanol concentration and the larger their radii.

Fluorescent lipids with similar chemical affinity to ethanol as monoolein, which are added to the ambient squalane phase, allow to trace the behavior of monoolein (Supplementary Movie 2). The sequence of micrographs in Fig. 2a reveals an influx of lipidic molecules from the ambient phase into the swimming droplet giving rise to a localized depletion zone around each droplet and a characteristic dark, i.e., monoolein-depleted, trail. Besides a depletion zone and a dark trail, which

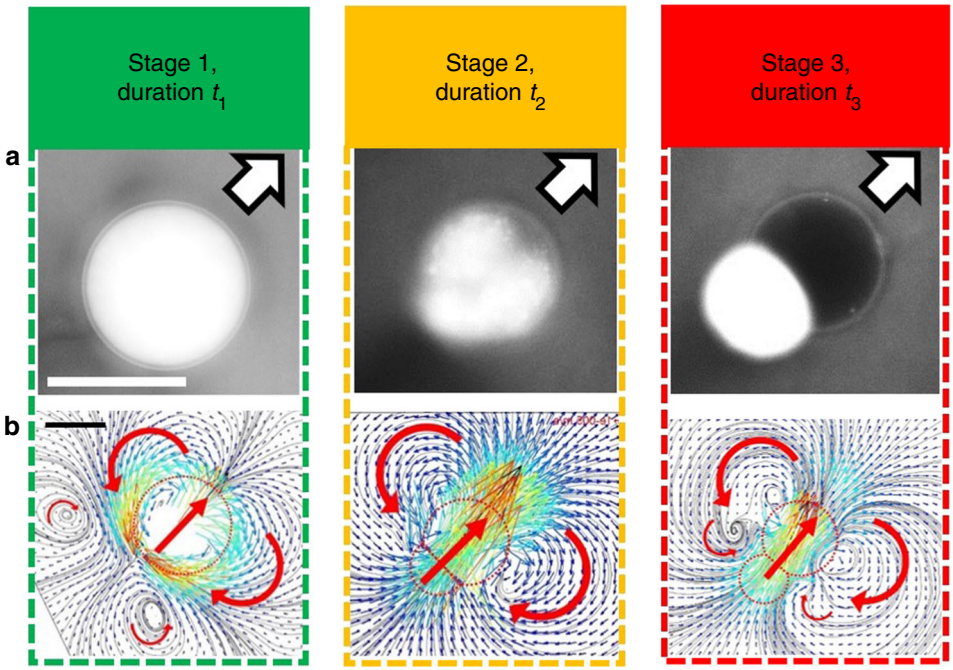

Fig. 2 Monoolein uptake and water/ethanol separation during droplet evolution as seen by fluorescence microscopy. **a** The fluorescent lipids were added to the squalane/monoolein solution and have a similar affinity to ethanol as to monoolein. From left to right: at stage 1, droplet appears bright due to the fluorescent lipid molecules taken up from the continuous phase. For the particular example of 80 vol% ethanol concentration additional dark regions are visible around the drop. At stage 2, the fluorescent lipids indicate the ethanol-rich phase during nucleation and coarsening (example 70 vol% ethanol). At stage 3, the fluorescent lipids indicate that the trailing droplet contains the ethanol-rich phase while the leading drop contains the water-rich phase in the Janus regime (example 70 vol% ethanol). **b** Flow fields around the self-propelling droplets in the different stages determined by μPIV in the co-moving frme of the droplete with 50 vol% ethanol. The droplets move close to the bottom surface of the device, that is about twice the height of the average droplet diameter. The flow fields were determined parallel to the bottom walls and are similar to the rotationally symmetric flow fields of: (from left to right) a weak pusher in stage 1, a neutral swimmer in stage 2, and a chain of neutral swimmers in stage 3. Scale bar is 100 μm

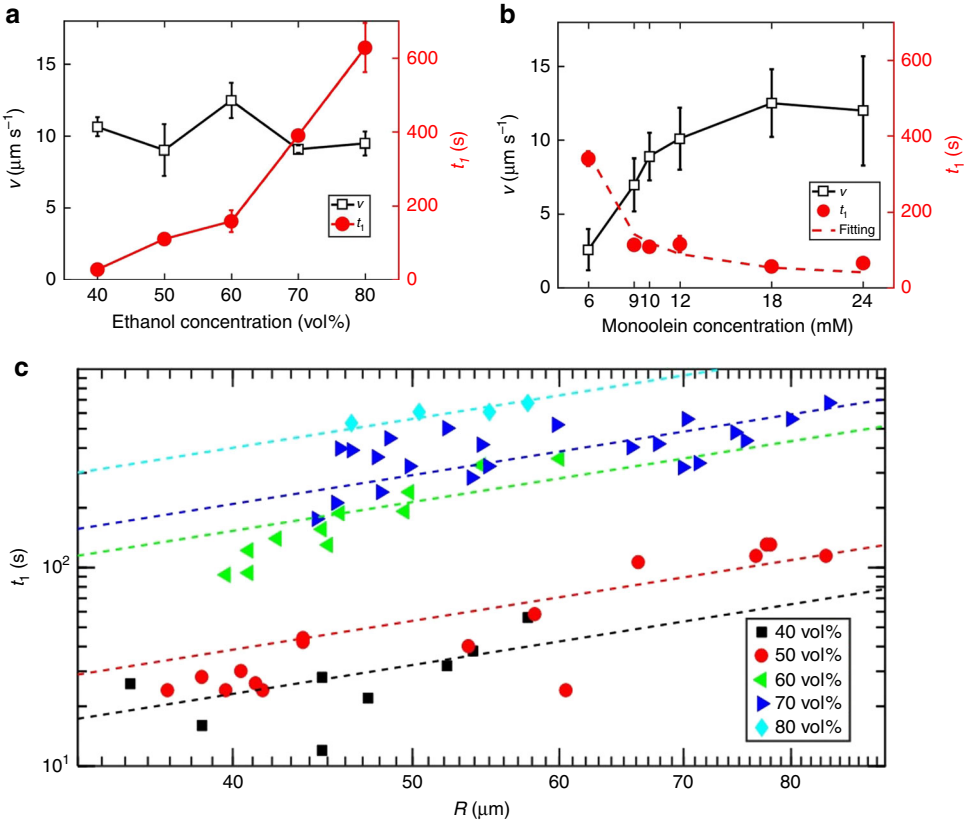

Fig. 3 Average droplet velocity and duration t_1 in stage 1. **a** As a function of ethanol concentration in the droplets at a fixed monoolein concentration of 10 mM in the surrounding squalane phase. **b** As a function of monoolein concentration in the surrounding squalane phase at a fixed ethanol concentration of 50 vol% in the droplet phase. The dashed line is the fit of Eq. (1). **c** Duration t_1 as function of droplet radius R for various initial ethanol concentration. The dashed lines indicate fits of Eq. (1) to the data with $\propto R^{3/2}$, where c^* is a free fitting parameter. Each point represents the mean value of several measurements while the corresponding error bar is the standard deviation

can be seen for all ethanol concentrations, dark clouds appear in the fluorescent micrograph for large ethanol concentrations $\gtrsim$70%, which are presumably related to Marangoni rolls[25]. The propulsion velocity increases with increasing monoolein concentration, while the duration t_1 of the propulsion in stage 1 is reduced, both reaching a plateau at a monoolein concentration of about 18 mM (Fig. 3b). Due to the opposing trends of propulsion velocity and duration with monoolein concentration, the total cruising range in stage 1 is hardly affected by the monoolein concentration. Note that we never observed self-propulsion or measured any volume loss for pure water droplets within the duration of an experiment.

Based on the findings above, we can conclude that the fraction of water leaving the droplets can be neglected with respect to the ethanol loss, and that ethanol solubilization in squalane drives the self-propulsion in stage 1. This mechanism has been described for liquid-crystal droplets[12,15], where molecules from the droplet phase are solubilized in a monoolein/squalane solution by loading the core of the surfactant micelles[10,12,14] leading to a variation of the surface tension at the droplet surface, and hence to a Marangoni flow[10,12,15]. However, the present situation is more complex, as substantial amounts of ethanol can be solubilized not only in the core of the micelles but also in the form of individual molecules in the squalane phase and thus the amount of solubilized ethanol is hard to predict. In line with the finite solubility of ethanol in squalane, we found droplet propulsion in stage 1 already at lower monoolein concentrations than reported in refs.[10–13,15] (Fig. 3a).

The hydrodynamic flow field around the droplets characterizes the active droplets in stage 1 as weak "pushers" (Fig. 2b), where pusher droplets are in a regime predicted by the squirmer model[26,27]. The symmetry of the corresponding flow field should result in characteristic long-range hydrodynamic interactions[26–28]. Based on their long-range hydrodynamic interactions, a pusher mode was already proposed for droplets driven by solubilization[15]. However, the observed flow fields was rather identified as a neutral squirmer (Fig. 2b)[11,15].

Controlled delay of the phase transition. Ethanol solubilization into the surrounding squalane phase and surfactant absorption from the squalane phase continue until small ethanol-rich droplets become visible inside the propelling droplet at the beginning of stage 2 (Figs. 1a, 2a). This observation is indicative of a spontaneous phase separation of the ternary mixture consisting of water, ethanol, and monoolein, as reported in literature[29–31], and sketched in the phase diagram in Fig. 1d. Following the shape of the single phase region in Fig. 1d, it is obvious why droplets with larger initial ethanol concentration have to loose more ethanol and are sustained longer in stage 1 before they reach the boundary of the single-phase region. Similarly, it is evident that the composition of the droplet reaches the boundary of the single-phase region earlier if more monoolein is present in the continuous phase and by the monoolein uptake determines the duration t_1 of stage 1 for a given ethanol concentration. In the following we will thus estimate t_1 as function of monoolein

concentration, which is given by the time when phase separation sets in.

The small extension of the monoolein-depleted region around a moving droplet relative to its size, as visible in Fig. 2a, indicates that we are operating at large Peclet numbers $\mathrm{Pe} = UR/D > 1$, where D is the diffusion constant of the monoolein molecules in the squalane phase, R the droplet radius, and U the velocity of self-propulsion. In this limit, we can employ the boundary-layer model of Levich[32] to calculate the adsorption rate of monoolein molecules, and thus the time to the onset of the phase separation marking the end of stage 1. Employing the estimated diffusion constant D for monoolein micelles in squalane from ref.[11] we arrive in fact at $\mathrm{Pe} \simeq 200$ for typical droplets with radius of $R = 50\,\mu\mathrm{m}$ and propelling velocity of $U = 10\,\mu\mathrm{m\,s}^{-1}$. For these conditions we can estimate the running time in stage 1 as:

$$t_1 = \sqrt{\frac{\pi}{6}}\frac{(1+\lambda)R^3}{DU}\frac{c^*}{c_\infty}, \qquad (1)$$

where c^* is the monoolein concentration in the droplet at the onset of phase separation. The ratio of dynamic viscosities of droplet and continuous fluid is abbreviated by λ. Here, we assumed that the monoolein concentration of the squalane phase at the surface of the leading droplet c_0 is much smaller than the bulk concentration c_∞, and consequently set $c_0 = 0$. The predicted scaling $t_1 \propto R^{3/2}$ is consistent with the experimental data for the various ethanol concentrations (Fig. 3c). Moreover, fitting Eq. (1) to the data shown in Fig. 3b and c for 50 vol% ethanol concentration, using the experimental determined droplet radii R, velocity U, viscosity ratio λ, and initial monoolein concentration c_∞, provides $c^* = (13 \pm 4)$ mM and $c^* = (8 \pm 3)$ mM, respectively. Assuming that the initial ethanol concentration of 50 vol% is reduced to 40–45 vol% at time t_1, the fitted values of c^* agree also with the occurrence of phase separation in the bulk.

According to the theoretical prediction and the experimental data, the duration t_1 of stage 1 can be controlled within two orders of magnitude by varying the monoolein concentration in the surrounding squalane phase, the ethanol concentration in the droplets and the droplet radius within a few ten to some hundred micrometer. The cruising range in stage 1, however, is hardly affected by the monoolein concentration but can be varied with ethanol concentration and droplet size, providing a handle for a temporally controlled cargo delivery.

Propulsion mechanism in stages 2 and 3. Following the shape of the single phase region in Fig. 1d, it is also clear that droplets with high ethanol concentration ($\gtrsim$70%) entering stage 2 reveal the formation and the growth of small water-rich droplets inside the propelling mother droplet. For such a high initial ethanol concentration, we find the formation of many small droplets of the water-rich minority phase decorating the droplet at the end of stage 2 (Fig. 1a). The change of the minority phase from the ethanol and monoolein-rich phase to the water and monoolein-poor phase clearly indicates the presence of a plait point on the boundary of the single phase region in Fig. 1d, where the interfacial tension of the coexisting phases vanishes. The observation that the minority phase droplets are eventually pushed out of the mother droplets is well in line with the expectation that the interfacial tension between the two coexisting ethanol-rich and water-rich phases increases as their relative concentrations move away from the plait point. Furthermore, the observation that the ethanol-rich minority droplets are fully engulfed by the water-rich phase shortly after their appearance suggests that the interfacial tension between the ethanol-rich phase and the squalane exceeds the interfacial tension between the water-rich phase and the squalane close to the plait point.

During phase separation, a continuous, almost linear increase of the propulsion velocity is observed (Fig. 1c), and the flow field emerging around a droplet in stage 2 is similar to that of a neutral squirmer (Fig. 3b)[26,27]. The simultaneously occurring swirl inside the droplet preferentially transports the coarsening small droplets toward the rear (Fig. 2). When the growing ethanol-rich droplet forms a three phase contact line with the droplet surface it is pushed out of the water-rich droplet forming a Janus droplet. This "budding" transition[33] is consistent with the general finding that the interfacial tension between two coexisting phases must increase as the concentrations move away from the plait point. The ethanol-rich droplet in contact with the surface of the water-rich droplet provides a sink (i.e., reduced chemical potential) for the monoolein molecules at the surface of the water-rich droplet. This gradient of the chemical potential contributes to a Marangoni flow that propels the droplet[34]. In the course of the coarsening process, when more of the small ethanol-rich droplets merge with the larger one, the depth of the sink increases which can explain the acceleration of the droplet propulsion. At the end of stage 2 droplets with initial ethanol concentrations ≤60% display a characteristic Janus morphology, consisting of a water-rich leading droplet that is in contact with an ethanol-rich trailing droplet. The latter contains the majority of monoolein molecules that have been previously taken up by the mother droplet. At the end of stage 2 no further nucleation of minority phase droplets is observed in the bulk of the leading droplet.

The velocity of the Janus droplet in stage 3 decreases exponentially until it reaches a constant, albeit small cruising velocity (Fig. 1c). The average propulsion duration for different ethanol concentrations in stage 3 is about 5 min with a mean velocity of about $5\,\mu\mathrm{m\,s}^{-1}$. The decreasing velocity in stage 3 can be qualitatively understood in terms of the chemical potential in the ethanol-rich droplet which represents a sink for monoolein molecule. The propulsion velocity is the larger the deeper the sink which decreases as more and more monoolein molecules are collected into the ethanol-rich droplet.

Also the evolution of the droplet morphology into a pronounced dumbbell shape toward the end of stage 3 including a final pinch-off of the trailing droplet is well in line with an increase of the interfacial tension between the water-rich and the ethanol-rich phase, as the relative concentrations of the two coexisting phases in Fig. 1d move away from the plait point. The flow field of the stable Janus droplets were identified as a chain of neutral swimmers, i.e., a dimer made of two neutral squirmers in contact (Fig. 2b)[26,27].

Spatial control of cargo delivery. The observed formation of Janus droplets by phase separation, the different wetting properties of the separated liquid phases, and the changing flow fields during the different evolution stages, whose duration can be controlled by chemical composition and droplet size, suggests itself to be used to accumulate certain molecules in one of the liquid phases and to use the formed Janus droplets as smart active carriers. The observed formation of Janus droplets allows to extract certain molecules into one of the liquids during phase separation. As we will demonstrate in the remainder of this work, the formed Janus droplets have the potential to be employed as smart active carriers for DNA molecules which accumulate in the ethanol-rich droplet during phase separation. Besides the kinetics of the phase separation and the different wetting properties of the liquid phases we exploit the changing flow fields during the different evolution stages to control the target location.

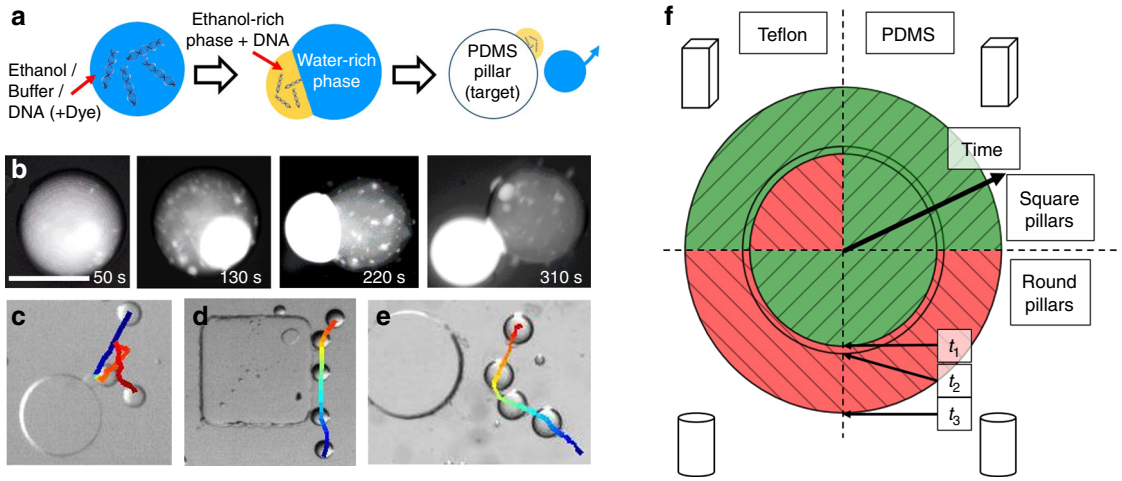

Fig. 4 DNA precipitation and controlled cargo delivery. **a** Sketch; the intensity of the blue and yellow colors indicate increasing concentration of water, respectively of ethanol. **b** Fluorescent microscopy time series showing the precipitation of fluorescent DNA into the ethanol-rich droplet, which finally pinches off. The initial droplet phase contained 50 vol% ethanol, 0.2 mg/ml DNA, 0.25 mg/ml Hoechst 33342, and 25 mg/ml sodium acetate. **c**–**e** Overlapped time series of droplets being hydrodynamically attracted to circular PDMS pillars in stage 1 and delivering cargo in stage 3 (**c**); attracted to square Teflon-coated pillars in stage 1, but not delivering cargo (**d**); and repelled from circular pillars in stage 3 (**e**). The shown traces denote 140 s (**c**), 180 s (**d**), and 50 s (**e**) from blue to red. The scale bars in **b** denote 100 μm, while the pillars in **c**–**e** are 800 μm across. **f** Sketch of possible delivery scenarios depending on target geometry and wettability. Green color (and left hashed) indicates attractive hydrodynamic interactions, while situations of repulsive hydrodynamic interactions are shown in red color (and right hashed). The top/bottom half sketches the situation for square and circular pillars, respectively, while the left/right half presents the situation for PDMS and Teflon surfaces

The sequence of images in Fig. 4a and b demonstrates the separation of fluorescing DNA from a water/ethanol droplet into an ethanol-rich droplet. The presence of salt reduces the DNA solubility in water, and therefore the DNA molecules precipitate and are extracted into the ethanol-rich droplet during the phase separation. It is worth emphasizing that, even in the presence of DNA and salt, the droplets undergo the previously described phase evolution and stages, and finally form Janus droplets consisting of a water-rich leading and an ethanol-rich trailing droplet. If the ethanol droplet of a randomly moving Janus droplet touches a target, the ethanol-rich phase may spread spontaneously on the surface. In this way the cargo molecules in the trailing droplet, like DNA, can be delivered to the target. As the examples in Fig. 4c–e demonstrate, the ability of a droplet to approach a target depends on both the geometric shape and the evolution stage, i.e., the squirmer mode, of a droplet.

Before phase separation, in stage 1, the active droplets are in a pusher mode, being attracted to circular pillars by virtue of their flow fields[28]. In case of Teflon-coated pillars, which are not wetted by the propelling water/ethanol droplets, the droplets can move in bound orbits around them[28]. In case of a circular PDMS pillar, however, the self-propelling droplets wet the pillar surface and remain attached to the point of first contact. When the ethanol-rich droplet is eventually formed at the end of stage 2 its flow field changes to that of a neutral swimmer, which is not attracted by a circular pillar any more. Thus, the water-rich droplet self-propels away from the circular Teflon-coated pillar, respectively, detaches from the circular PDMS pillar, which inevitably brings the ethanol-rich droplet in contact with the pillar. And as the interface between the ethanol-rich droplet and the squalane forms a small equilibrium contact angle with both a Teflon and a PDMS surface, it spreads at both circular pillars made of PDMS or Teflon and deposits its cargo (Fig. 4c). A self-propelling Janus droplet in stage 3, which had not been previously captured by a pillar in stage 1, exhibits a long-range hydrodynamic repulsion with circular pillars. So no target can be approached in stage 3 and thus no cargo can be delivered (Supplementary Movie 3). According to this behavior, the cargo delivery time to circular pillars can be estimated by the sum of the duration of stage 1, t_1, which depends on ethanol concentration, monoolein concentration, and droplet size and the duration of stage 2, $t_2 \approx 90$ s, which is about constant for the various tested experimental conditions. Similarly, the maximum cargo delivery distance can be estimated by this duration multiplied with the average swimming velocity in stage 1 of about $U \approx 10\,\mu\mathrm{m\,s}^{-1}$.

Because of long-range hydrodynamic interactions of the pusher droplets with square pillars, the active droplets are attracted to square pillars also in stage 1[35,36]. In case of Teflon pillars, the droplets move along their side walls, but might leave them when approaching a corner (Fig. 4d). When approaching a square PDMS pillar in stage 1, the droplet will remain fixed at the point of first contact and eventually deliver its cargo at the end of stage 2, as explained previously for circular PDMS pillars (Supplementary Movie 3). However, Janus droplets obeying the flow field of neutral swimmer in stage 2 and stage 3 will be attracted to square pillars when approaching a straight wall[35,36] and will deliver their cargo contained in the ethanol-rich droplet irrespective of the pillar surface. In contrast to circular pillars, where the delivery time is a fairly small time interval around $t_1 + t_2$, the same time is a lower threshold for cargo delivery at square pillars. Accordingly, also the transport distance can be significantly larger when square pillars are the designated targets.

The different capture scenarios are sketched in Fig. 4f for square and circular pillars with a PDMS or Teflon surface. Cargo delivery will be obtained whenever a droplet is attracted by a pillar and either remains at a pillar until entering the Janus state or when a Janus droplet is attracted by a target location (Supplementary Movie 3).

Discussion

In this work we present self-propelled droplets, which are able to deliver cargo at specific targets. Even though all results presented above were obtained for water/ethanol droplets in a surrounding monoolein/squalane solution, these type of droplets can be

produced also for a large number of combinations of alcohols (including liquors), oils, and amphiphilic molecules. The process of controlled cargo delivery relies on the sequence of propulsion mechanism that change between different evolution stages. Each propulsion mechanism generates a certain hydrodynamic flow field around a droplet, evolving from a weak pusher in stage 1 over a neutral swimmer in stage 2 to a dimer of neutral swimmers in stage 3. These hydrodynamic flow fields determine the long-range hydrodynamic interactions with the possible targets, enabling a selectivity of target geometry. Curved walls attract droplets only in stage 1, while flat walls attract droplets in all three stages. Cargo is delivered if the short-range interactions, controlled by the wettability, promote spreading of the cargo containing droplet on the target.

The onset of de-mixing determines the duration of stage 1, which is controlled by the ethanol concentration in the droplets, the surfactant concentration in the surrounding oil phase, and the volume of the droplets. The cruising range in stage 1, however, depends solely on ethanol concentration and droplet volume. This implies that the droplet chemical composition provides a temporal control of the time cargo delivery while the spatial control is provided by a combination of the emerging flow fields in each evolution stage, target geometry, and surface wettability. We demonstrated this spatiotemporal controlled cargo delivery using droplets with radius of 30 μm and 40% ethanol concentration, which separate and deliver DNA at circular pillars after about 20 s and a maximum travel distance of about 200 μm. Larger droplets with 80 μm radius and an ethanol content of 70% deliver cargo at square PDMS pillars within almost 800 s and within a range of about 5 mm.

The combination of this programmable active carrier droplets with optimized microfluidic protocols may allow conducting novel tasks in an automated manner while manipulating tiny liquid volumes. In particular we expect that these programmable active droplets open new perspectives for droplet-based digital PCR[37], sorting of biomolecules according to reaction time like polymerization, DNA replication or protein expression[38], and possibly genes, drugs or nutrients delivery into cells[39].

Methods

Microfluidic chambers. To fabricate the observation chambers with flat bottom, glass slides were cut into squares of about 2.5 × 2.5 cm^2 and coated with octadecyltrichlorosilane (OTS), from Sigma, using the recipes published in ref. [40,41]. The OTS-coated glass squares were stacked with a cover slide (thickness 150 μm) as a spacer and glued together at three sides using epoxy glue. The observation chambers with pillar structures were fabricated by closing a PDMS (Sylgard 184, Dow Corning) pattern with a OTS-coated glass square. The PDMS pattern was fabricated by molding against a micro-machined negative master containing the pillar arrays. To reduce the surface energy of the cured PDMS structure, it was Teflon coated prior to closing with the OTS-coated glass substrate. Teflon coating was achieved by dip coating the PDMS pattern in a FC-72 (3M) solution containing 0.4% AF2400 (Sigma). Subsequently the Teflon solution was cured on a on hot plate at 70 and 270 °C for 10 min, each.

Active droplet production. To conduct an experiment (all experiments were conducted at room temperature), the observation chamber is pre-filled with an oil/surfactant mixture before an ethanol/water mixture is carefully injected into the reservoir using a glass capillary (20 μm inner diameter that is connected to a syringe pump). Droplets of variable radius between 30 and 80 μm were formed while the water/ethanol mixture was ejected from the glass capillary by adjusting the flow volume. Additionally, the size of the produced droplets could be controlled by changing the inner diameter of the glass capillary. The density of the aqueous phase was always higher than that of the oily phase (0.81 g/ml), even for the highest ethanol concentration (80 vol.%) used. The concentration of monoolein was fixed to 3.5 mg/ml (i.e., about 10 mM), if not explicitly mentioned otherwise. In each experiment, the large majority of droplets self-propels. Only a small fraction of the droplets is not moving, presumably because they stick to impurities on the chamber bottom. As mentioned in the main text, it is possible to extend the production to other chemical compositions: as examples, ethanol could be replaced by isopropanol, methanol or water/ethanol mixtures can be replaced by liquors with an alcohol content of 40 vol% (gin, whisky, vodka). And monoolein can be replaced by Span80 (Sigma), DOPC (1,2-dioleoyl-sn-glycero-3-phosphocholine), or DPhPC (1,2-diphytanoyl-sn-glycero-3-phosphocholine) from Avanti Polar Lipids. The oil can be replaced by squalene oil (Sigma). Droplets in these alternative systems are always self-propelling in stage 1 and, depending on their exact chemical composition, may produce Janus droplet (or phase transition) obeying the same typical behavior in stages 2 and 3 as described in the main text.

Lipids and DNA. All chemicals were purchased from Sigma-Aldrich, except the fluorescent lipid (1,2-dipalmitoyl-sn-glycero-3-phosphoethanolamine-N-7-nitro-2-1,3-benzoxadiazol-4-yl; CAS Number: 810144P), which was purchased from Avanti Polar Lipids. For the DNA cargo delivery experiments, the droplet phase was an ethanol/water mixture (50 vol.%) containing 0.2 mg/ml DNA (single-strand DNA from herring sperm), 0.25 mg/ml of a fluorescence dye (Hoechst 33342) forming a compound with the DNA and 25 mg/ml sodium acetate. DNA and sodium acetate were purchased from Sigma-Aldrich.

Data availability. The datasets generated and/or analyzed during the current study are available with the following https://doi.org/10.6084/m9.figshare.6198497.

Received: 31 January 2018 Accepted: 8 May 2018
Published online: 07 June 2018

References

1. Parmar, J. et al. Nano and micro architectures for self-propelled motors. *Sci. Technol. Adv. Mater.* **16**, 014802 (2015).
2. Baylis, J. R. et al. Self-propelled particles that transport cargo through flowing blood and halt hemorrhage. *Sci. Adv.* **1**, 9 (2015).
3. Wang, J. *Nanomachines: Fundamentals and Applications* (Wiley-VCH, Weinheim, 2013).
4. Purcell, E. M. Life at low Reynolds-number. *Am. J. Phys.* **45**, 11 (1977).
5. Lauga, E. Life around the scallop theorem. *Soft Matter* **7**, 3060–3065 (2011).
6. Michelin, S., Lauga, E. & Bartolo, D. Spontaneous autophoretic motion of isotropic particles. *Phys. Fluids* **25**, 061701 (2013).
7. Jiang, S. et al. Janus particle synthesis and assembly. *Adv. Mater.* **22**, 1060–1071 (2010).
8. Xuan, M. et al. Self-propelled Janus mesoporous silica nanomotors with sub-100 nm diameters for drug encapsulation and delivery. *Chem. Phys. Chem.* **15**, 2255–2260 (2014).
9. Li, J. et al. Self-propelled nanomotors autonomously seek and repair cracks. *Nano Lett.* **15**, 7077–7085 (2015).
10. Seemann, R., Fleury, J. -B. & Maass, C. Self-propelled droplets. *Eur. Phys. J. Spec. Top.* **225**, 2227–2240 (2016).
11. Thutupalli, S., Seemann, R. & Herminghaus, S. Swarming behavior of simple model squirmers. *New J. Phys.* **7**, 073021 (2011).
12. Peddireddy, K. et al. Solubilization of thermotropic liquid crystal compounds in aqueous surfactant solutions. *Langmuir* **28**, 12426 (2012).
13. Izri, Z. et al. Self-propulsion of pure water droplets by spontaneous Marangoni-stress-driven motion. *Phys. Rev. Lett.* **113**, 248302 (2014).
14. Maass, C., Kruger, C., Herminghaus, H. & Bahr, C. Swimming droplets. *Annu. Rev. Condens. Matter Phys.* **7**, 6.1–6.23 (2016).
15. Herminghaus, S., Maass, C., Thutupalli, S. & Bahr, C. Interfacial mechanisms in active emulsions. *Soft Matter* **10**, 7008 (2014).
16. Thakur, S., Kumar, P. S., Madhusudana, N. & Pullarkat, P. A. Self-propulsion of nematic drops: novel phase separation dynamics in impurity-doped nematogens. *Phys. Rev. Lett.* **97**, 115701 (2006).
17. Poesio, P., Beretta, G. & Thorsen, T. Dissolution of a liquid microdroplet in a nonideal liquid-liquid mixture far from thermodynamic equilibrium. *Phys. Rev. Lett.* **103**, 064501 (2009).
18. Ban, T., Aoyama, A. & Matsumoto, T. Self-generated motion of droplets induced by Korteweg force. *Chem. Lett.* **39**, 1294–1296 (2010).
19. Ban, T., Yamada, T., Aoyama, A., Takagi, Y. & Okano, Y. Composition-dependent shape changes of self-propelled droplets in a phase-separating system. *Soft Matter* **8**, 3908 (2012).
20. Bormashenko, E. et al. Janus droplets: liquid marbles coated with dielectric/semiconductor particles. *Langmuir* **27**, 7–10 (2011).
21. Jeong, J. et al. Liquid crystal Janus emulsion droplets: preparation, tumbling, and swimming. *Soft Matter* **11**, 6747–6754 (2015).
22. Choi, C. H., Weitz, D. A. & Lee, C.-S. One step formation of controllable complex emulsions: from functional particles to simultaneous encapsulation of hydrophilic and hydrophobic agents into desired position. *Adv. Mater.* **25**, 2536–2541 (2013).

23. Guzowski, J. et al. The structure and stability of multiple micro-droplets. *Soft Matter* **8**, 7269–7278 (2012).
24. Li, W. et al. Controllable microfluidic fabrication of Janus and microcapsule particles for drug delivery applications. *RSC Adv.* **5**, 23181 (2015).
25. Schwarzenberger, K. Pattern formation and mass transfer under stationary Marangoni instability. *Adv. Coll. Interf. Sci.* **206**, 344–371 (2014).
26. Blake, J. R. A spherical envelope approach to ciliary propulsion. *J. Fluid Mech.* **46**, 199 (1971).
27. Lighthill, M. J. On the squirming motion of nearly spherical deformable bodies through liquids at very small Reynolds numbers. *Commun. Pure Appl. Math.* **2**, 109–118 (1952).
28. Spagnolie, S. E., Moreno-Flores, G. R., Bartolo, D. & Lauga, E. Geometric capture and escape of a microswimmer colliding with an obstacle. *Soft Matter* **11**, 3396–3411 (2015).
29. Efrat, R. et al. Liquid micellar discontinuous cubic mesophase from ternary monoolein/ethanol/water mixtures. *Colloids Surf. A* **299**, 133–145 (2007).
30. Spicer, P. T. et al. Novel process for producing cubic liquid crystalline nanoparticles (cubosomes). *Langmuir* **17**, 5748 (2001).
31. Engstrom, S., Alfons, K., Rasmusson, M. & Ljusberg-Wahren., H. Solvent-induced sponge (L_3) phases in the solvent-monoolein-water system. *Progr. Colloid Polym. Sci.* **108**, 93–98 (1998).
32. Levich, V. G. *Physicochemical Hydrodynamics*(Prentice-Hall, Englewood Cliffs, NJ, 1962).
33. Dimova, R. & Lipowsky, R. Wetting-induced budding of vesicles in contact with several aqueous phases. *Soft Matter* **8**, 6409 (2012).
34. Hyoungsoo, K., Muller, K., Shardt, O., Afkhami, S. & Solutal Marangoni flows of miscible liquids drive transport without surface contamination *Nat. Phys.* **13**, 1105–1110 (2017).
35. Li, G. -J. & Ardekani, A. M. Hydrodynamic interaction of microswimmers near a wall. *Phys. Rev. E* **90**, 013010 (2014).
36. Simmchen, J. et al. Topographical pathways guide chemical microswimmers. *Nat. Commun.* **7**, 10598 (2016).
37. Hindson, C. M. Absolute quantification by droplet digital PCR versus analog real-time PCR. *Nat. Methods* **10**, 1003–1005 (2013).
38. Neal, A. E. & Goldup, S. M. A kinetic self-sorting approach to heterocircuit [3] rotaxanes. *Angew. Chem. Int. Ed.* **55**, 12488–12493 (2016).
39. Chiu, F. W. Y. et al. A microfluidic toolbox for cell fusion. *J. Chem. Technol. Biotechnol.* **91**, 16–24 (2015).
40. Sagiv, J. Organized monolayers by adsorption. 1. Formation and structure of oleophobic mixed monolayers on solid surfaces. *J. Am. Chem. Soc.* **102**, 95–98 (1980).
41. Lessel, M. et al. Self-assembled silane monolayers: an efficient step-by-step recipe for high-quality low energy surfaces. *Surf. Interf. Anal.* **47**, 557–564 (2015).

Acknowledgements

M.L., M.B., and R.S. acknowledges funding from SPP1726.

Author contributions

M.L. performed the experiments and analyzed the data. M.B. developed the theory. M.L., M.B., R.S., I.P., and J.-B.F. discussed the results. M.L., M.B., R.S., and J.-B.F. wrote the paper. M.B., R.S., and J.-B.F. directed the research. J.-B.F. designed the research.

Additional information

Supplementary information accompanies this paper at https://doi.org/10.1038/s42005-018-0025-4.

Competing interests: The authors declare no competing interests.

Reprints and permission information is available online at http://npg.nature.com/reprintsandpermissions/

Publisher's note: Springer Nature remains neutral with regard to jurisdictional claims in published maps and institutional affiliations.